Enhanced densification of Ti-6Al-4V/TiC powder blends by transformation mismatch plasticity

Bing Ye
National Engineering Research Center of Light Alloy Net Forming and State Key Laboratory of Metal Matrix Composites, School of Materials Science and Engineering, Shanghai Jiao Tong University, Shanghai 200240, China; and Department of Materials Science and Engineering, Northwestern University, Evanston, Illinois 60208

Marc R. Matsen
Boeing Research and Technology, The Boeing Company, Seattle, Washington 98124

David C. Dunand[a)]
Department of Materials Science and Engineering, Northwestern University, Evanston, Illinois 60208

(Received 27 January 2013; accepted 29 March 2013)

Ti-6Al-4V alloy with attractive properties such as corrosion resistance and high specific strength has a broad impact on daily life in the field of aerospace and medicine. The addition of TiC to Ti-6Al-4V is to further improve abrasion resistance and hardness. To have a low processing cost and precise control of the TiC volume fraction and distribution, the composite is densified with a blend of Ti-6Al-4V and TiC powders through a powder metallurgy route. The densification kinetics of the blend is studied for uniaxial die pressing (i) under isothermal conditions at 1020 °C, where β-Ti-6Al-4V deforms by creep and (ii) upon thermal cycling from 860 to 1020 °C, where the α-β transformation leads to transformation superplasticity. Densification curves for both isothermal and thermal cycling for various applied stresses and TiC fractions are in general agreement with predictions from continuum models and finite element simulation models performed at the powder level.

I. INTRODUCTION

Ti-6Al-4V, the workhorse titanium alloy for aerospace and medical applications, has attractive properties, including excellent corrosion resistance and biocompatibility as well as high specific strength and stiffness.[1–3] These mechanical properties, as well as abrasion resistance and hardness, can further be improved by incorporation of stable reinforcing ceramic particles such as TiC with high modulus and hardness.[4–6] Titanium metal-matrix composites are usually processed by powder metallurgy, using pressure to densify metal/ceramic blends via hot pressing, hot isostatic pressing, or extrusion.[4,7–9] Since residual porosity adversely affects ductility of these and most other MMCs, the densification of titanium/ceramic powder blend has been the subject of various studies. Densification modeling using continuum approaches[7,10–13] considers plastic deformation of individual powders in the initial stage (for a relative density of up to 90%), and the collapse of individual pores within a continuous matrix in the final stage (for a relative density above 90%). Usually, densification occurs at constant temperature where the main mechanism for powder deformation is dislocation (or power-law) creep.[7,10–12] Ti-6Al-4V has a reversible transformation between its α and β phases, which spans a wide range of temperatures but occurs principally from 860 to 1000 °C.[14] Enhanced densification kinetics of Ti-6Al-4V powders can be obtained during hot pressing while cycling about the phase transformation range of Ti-6Al-4V,[15] as it activates transformation-mismatch plasticity which is a deformation mechanism more rapid than dislocation creep at low stresses.[13,16–19] Powder densification modeling has been extended to transformation-mismatch plasticity of pure Ti and Ti-6Al-4V powders[13,14] and Ti with zirconia powder reinforcement.[13] In the latter case however, chemical reaction between the metal and the ceramic inhibited the densification and made the modeling difficult. A better choice of ceramic reinforcement is titanium carbide, which is at chemical equilibrium with Ti and Ti-6Al-4V.

We present here an experimental study of densification of blends of Ti-6Al-4V and TiC powders under thermal cycling (860–1020 °C) where the transformation plasticity is dominant in Ti-6Al-4V or isothermal conditions (at 1020 °C) where dislocation creep controls the deformation of β-Ti-6Al-4V. These experimental densification kinetics data are compared to predictions from continuum models and finite element (FE) simulations.

[a)]Address all correspondence to this author.
e-mail: dunand@northwestern.edu
DOI: 10.1557/jmr.2013.95

II. EXPERIMENTAL PROCEDURES

A. Materials

Spherical Ti-6Al-4V powders produced by the plasma rotating electrode process were purchased from Starmet Corp. (Concord, MA). These ELI (Extra Low Interstitial) Ti-6Al-4V powders had a size of ~80 μm [Fig. 1(a)] and the following composition (in wt%, as provided by the supplier): 6.07% Al, 3.81% V, 0.192% O, 0.18% Fe, 0.02% C, 0.02% Si (ASTM F136). Angular TiC powders, purchased from CERAC, Inc. (Milwaukee, WI), had a size of ~44 μm (−150/+325 mesh) and contained high porosity, as shown in Fig. 1(b). Since in this work, the only concern was consolidation kinetics of the Ti-6Al-4V matrix, TiC porosity was not considered a problem; however, fully dense TiC powders would be beneficial to MMC used in load-bearing applications.

The Ti-6Al-4V/TiC blends with target TiC volume fractions 5, 10, 15, and 20% were prepared by measuring specific masses of Ti-6Al-4V and TiC rather than volumes, assuming TiC and Ti-6Al-4V densities of 4.93 and 4.43 g/cm^3, respectively. The TiC powder was however found to have an intrinsic porosity of 28.6% from both image analysis and data analysis, as described in the following section. The nominal (dense) TiC volume fractions of 5, 10, 15, and 20% in the composites thus correspond to higher actual (porous) TiC volume fractions of 6.8, 13.5, 19.8, and 25.9% (rounded to 7, 14, 20, and 26%).

B. Composite densification

The Ti-6Al-4V and TiC powders were thoroughly blended in a custom-made cylinder container with a single axially-located baffle.[20,21] The hot pressing procedure is described in detail in Ref. 15 and is summarized here. 14.5–15.5 g of Ti-6Al-4V/TiC powder blend was poured in a cylindrical TZM molybdenum alloy die coated with boron nitride, with inner and outer diameters of 25.4 and 63.5 mm, and a height of 34.3 mm. Powders were not tapped to avoid possible segregation. Both TZM piston and die walls were separated from the powder by two 125 μm thick stainless steel foils coated with boron nitride. The powder temperature was monitored by a K-type thermocouple in contact with the center of the TZM piston.

The evacuated TZM die/powder/piston assembly was induction-heated from ambient to densification temperature at a heating rate of ~1 K/s, with the powders subjected to a small compressive stress of ~0.4 MPa to maintain load train continuity. In the isothermal experiments, the densification stress was applied to the powders when the temperature reached 1020 °C (in the β-field of Ti-6Al-4V) and the stress and temperature were maintained constant throughout the experiment. In the thermal cycling experiments, the densification stress was applied when the temperature reached 850 °C at which point the stress remained constant while the temperature was cycled between 860 and 1020 °C with a heating time of 96 s and a cooling time of 95 s (i.e., ~3 min cycle). At these lower and upper temperatures, the equilibrium volume fraction of β-phase is 22 and 100%, respectively.[14] A vacuum level of at least 5×10^{-5} Torr (6.7 mPa) was maintained throughout the experiment. The temperature was recorded every 2 s, together with the piston displacement measured at the cross-head by a displacement transducer with an accuracy of ±3 μm. At the end of densification, the sample was cooled under a small ~0.4 MPa stress in a vacuum to room temperature within 2 h.

The density of the sample, with a height of ~7 mm and a diameter of 25.4 mm, was measured by the Archimedes method in deionized water. The sample relative density (with an error about 0.3%) during the densification experiment was then calculated using the measured final density and the piston displacement data. Densification was conducted for each Ti-6Al-4V/TiC blend with different TiC volume fraction and densification kinetics was measured on separate sample for each blend condition. Metallographic samples were prepared as described in Ref. 15.

III. RESULTS

A. Microstructure and composite density

The microstructure of the densified composite with the highest TiC volume fraction (26 vol%) is shown in

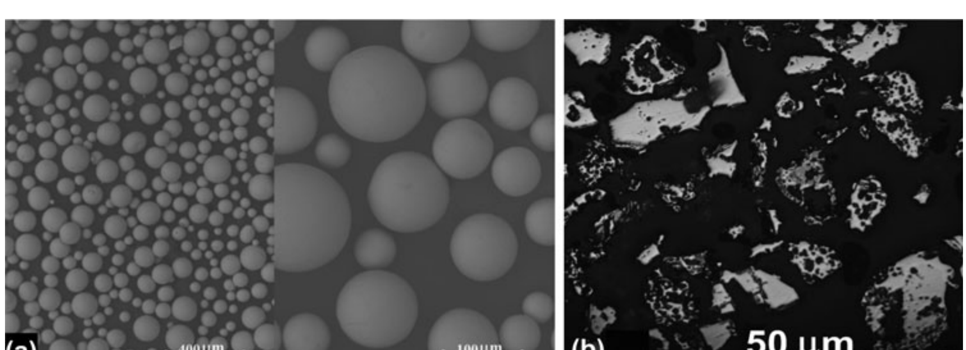

FIG. 1. SEM images of (a) spherical Ti-6Al-4V powders and (b) angular, porous TiC powders polished in the cross-section.

Figs. 2(a) and 2(b) after densification at 1020 °C under 20 MPa for 7500 s. A low-magnification cross-section [Fig. 2(a)] shows a uniform distribution of TiC particles, even near the edge of the die [marked by arrows in Fig. 2(a)]. A high-magnification cross-section [Fig. 2(b)] shows an intimate contact between matrix and particles and the absence of the reaction product, as expected. A Widmanstätten or "basket weave" structure is visible in the Ti-6Al-4V phase, as well as extensive porosity within the TiC powders [Fig. 2(b)].

Figure 2(b) and all other metallographic sections show that the rigid TiC particles were not crushed during densification below 20 MPa and maintained their high initial porosity. This suggests that TiC is rigid during the densification with an applied stress below 20 MPa. The apparent density of the porous TiC powders was determined by plotting the measured density of four fully densified composites against their nominal TiC volume fractions (5, 10, 15, and 20%). The resulting straight line yields an apparent TiC density of 3.52 g/cm^3, corresponding to a TiC porosity of 28.6%. Image analysis of cross-sections of individual TiC particles confirmed this value.

B. Thermal cycling and isothermal densification

Densification curves (relative density versus time) for blends with TiC volume fractions of 0, 7, 14, 20, and 26% densified under thermal cycling conditions (860–1020 °C) at 10 and 20 MPa applied stress are shown in Figs. 3(a) and 3(b), respectively. Similar densification curves for isothermal densification at 1020 °C for 10 and 20 MPa are shown in Figs. 4(a) and 4(b), respectively for 0, 14, and 26% TiC. Under thermal cycling conditions [Figs. 3(a) and 3(b)], addition of 7 vol% TiC strongly delays densification kinetics as compared to pure Ti-6Al-4V; increasing the TiC volume fraction further to 14, 20, and 26% leads to a comparatively much smaller retarding effect. By contrast, under isothermal conditions [Figs. 4(a) and 4(b)], the presence of 14 vol% TiC affects the densification kinetics, as compared to TiC-free powders, only at the start of densification, but the times to achieve full densification are similar. When the TiC volume fraction is 26%, the decrease in densification kinetics is however very significant, particularly at the lower stress of 10 MPa.

During thermal cycling, densification is controlled by transformation-mismatch plasticity which is proportional to the mismatch occurring during the α/β transformation of Ti-6Al-4V and thus the range of β-phase variation. As expected, Fig. 5 shows that partial cycling (860–984 °C), which corresponds to the equilibrium volume fraction of β-phase of 22 and 90%, respectively,[14] results in lower densification kinetics than full cycling (860–1020 °C, or 22–100% β-phase).

IV. DISCUSSION

A. Powder densification under thermal cycling and isothermal conditions

Under thermal cycling, when deviatoric stresses are low, densification occurs primarily by transformation-mismatch plasticity while, under isothermal conditions, power-law dislocation creep is the dominant deformation mechanism. For a bulk material subjected to an uniaxial stress σ_x, the average strain rate $\dot{\varepsilon}$ due to creep under isothermal conditions is:

$$\dot{\varepsilon} = C \cdot \sigma_x{}^n \quad , \tag{1}$$

where n is the creep stress exponent (for β-Ti-6Al-4V) and C is a constant incorporating an Arrhenius temperature dependence: for Ti-6Al-4V, $C = 4.8 \times 10^{-7}$ MPa$^{-2.8}$/s at 1020 °C[14,22] with $n = 2.8$,[22] while for Ti, $C = 3.86 \times 10^{-9}$ MPa$^{-4.3}$/s at 870 °C and $C = 6.74 \times 10^{-6}$ MPa$^{-4.3}$/s at 980 °C with $n = 4.3$[7,23,24]. Similarly, the average uniaxial strain rate $\bar{\dot{\varepsilon}}$ due to transformation-mismatch plasticity under thermal cycling is[16]:

$$\bar{\dot{\varepsilon}} = \frac{4}{3} \cdot \frac{5 \cdot n}{4 \cdot n + 1} \cdot \frac{\Delta V}{V} \cdot \frac{1}{\Delta t} \cdot \frac{\sigma_x}{\sigma_0} \quad , \tag{2}$$

where $\Delta V/V$ is the volume mismatch for full α/β phase transformation ($\Delta V/V = 0.96\%$ for Ti-6Al-4V[14]), Δt is the

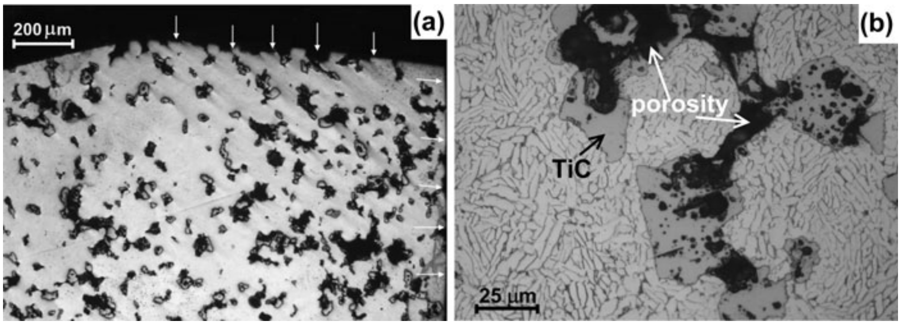

FIG. 2. Cross-sections of densified Ti-6Al-4V/20TiC composites with the loading direction oriented vertically: (a) low magnification showing overall distribution of TiC particles (edge of the composite marked by arrows), (b) high magnification with etched Ti-6Al-4V microstructure (TiC particles and porosities from sintering are marked by arrows).

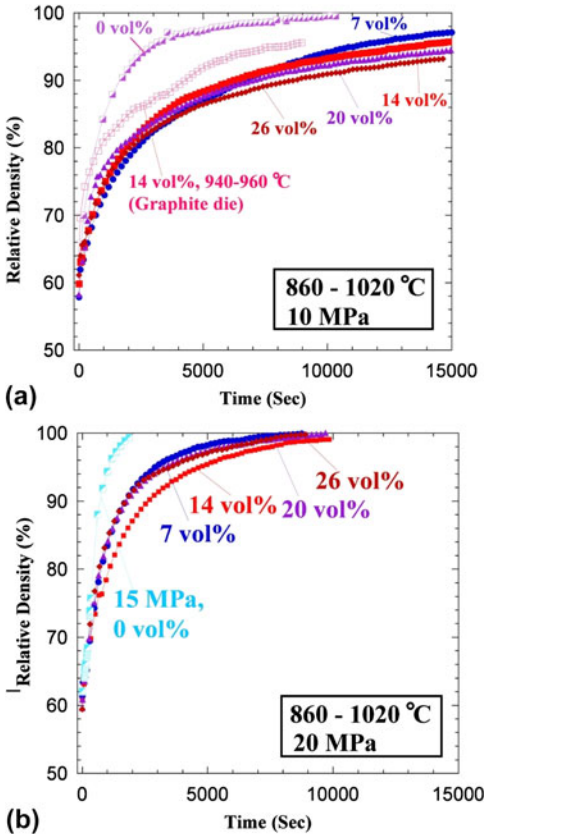

FIG. 3. Powder densification kinetics of Ti-6Al-4V with various TiC fractions under thermal cycling densification (860–1020 °C) with an applied stress of (a) 10 MPa and (b) 20 MPa.

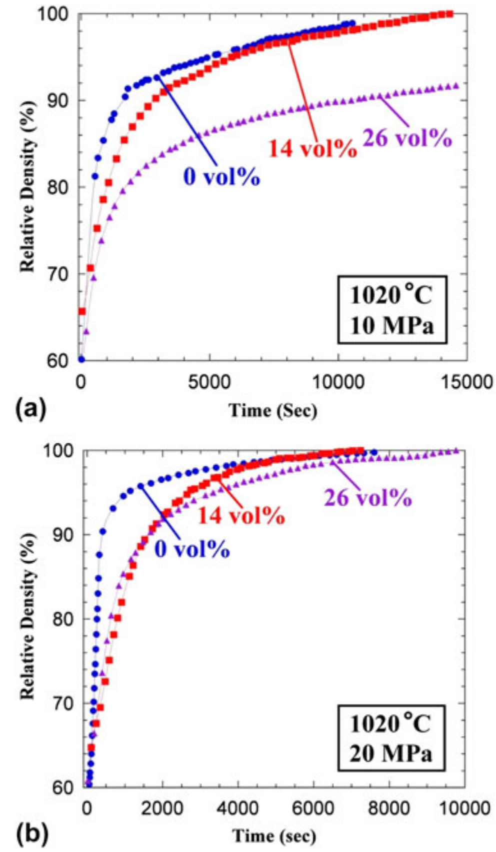

FIG. 4. Powder densification kinetics of Ti-6Al-4V with various TiC fractions under isothermal densification (1020 °C) with an applied stress of (a) 10 MPa and (b) 20 MPa.

thermal cycle duration from heating and cooling and σ_0 is the average internal stress generated during the phase transformation (σ_0 = 7.4 MPa for Ti-6Al-4V[14]).

In dense composites, the uniaxial strain rate from dislocation creep is significantly reduced by rigid reinforcing ceramic particles due to the constrained matrix flow and load transfer from the matrix to the rigid particles (when there is good bonding between the two phases).[25,26] For transformation superplasticity, additional mismatch between the transforming matrix and the non-transforming matrix can enhance the creep rate of composites.[27–31] For densification of metal-ceramic powder blends, addition of rigid ceramic particles reduces densification rates under isothermal conditions, where powders deform by creep, due to the constraining effect of the ceramic particles on the creep deformation of the metal powders[7,13,32]; furthermore, at high reinforcement fractions, the presence of a load-bearing percolating network of ceramics can strongly inhibit metal densification. Although the densification rates of blends of Ti powders with 1, 5, or 10 vol% ZrO_2 particles were higher under thermal cycling than under isothermal conditions, the densification kinetics of the 5 and 10 vol% ZrO_2 blends were typically much reduced as compared to those of pure Ti.[7,13] This was attributed to

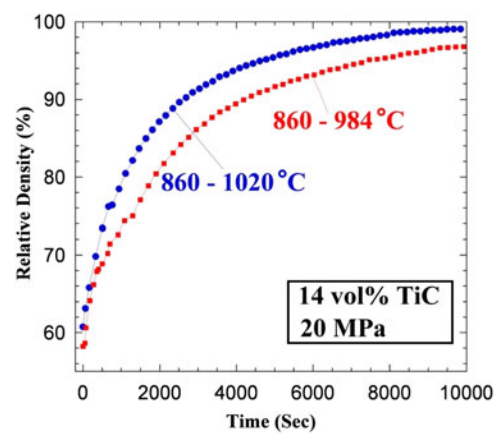

FIG. 5. Powder densification kinetics of Ti-6Al-4V with 14 vol% TiC composite under thermal cycling densification (860–984 °C and 860–1020 °C).

the dissolution of the ZrO_2 particles which strengthens the Ti matrix and prevents phase transformation.[7,13]

The percolation effect becomes important in a metal matrix composite only when the volume fraction is above 30% or so.[33,34] However, even when the volume fraction is low as much as 5%, the reduced densification

kinetics was observed.[34] The delay in densification kinetics is not significantly affected by the percolation effect and elastic constants of the rigid particles, but the friction effect between the powders[33] which is equivalent to lower applied stress.

An additional issue associated with composite densification during thermal cycling is the thermal conductivity of the ceramic reinforcement. While thermal conductivity of titanium and Ti-6Al-4V increases with temperature and is 20–25 W/(m·K) above 800 °C, the thermal conductivity of ceramics typically decreases with temperature and are 5.6 W/(m·K) for TiC[35] and 2 W/(m·K) for ZrO_2[36] above 800 °C. The ceramic powders thus reduce the heat transfer from and to the die, resulting in thermal gradients in the preform and thus gradients in thermal amplitude (and mismatch and transformation superplasticity), which reduce overall densification.

B. Continuum modeling of Ti-6Al-4V/TiC densification

Modeling of powder densification includes the first stage (for relative density $\rho < 90\%$) and the final stage (for relative density $\rho > 90\%$). Under isothermal conditions, the first-stage densification rate $\dot{\rho}$ based on power-law dislocation creep [Eq. (1)] can be expressed as[11,13,15]:

$$\dot{\rho} = 3.06 \cdot C \cdot \left(\frac{1-\rho_0}{\rho-\rho_0}\right)^{n-1/2} \cdot \frac{\rho_0^{1/3}}{\rho^{2n-2/3}} \cdot \left(\frac{B_i \cdot \sigma}{3}\right)^n \quad , \tag{3}$$

where σ is the uniaxial applied stress on the die piston, $B_i = 1.1$[13] is a dimensionless constant taking into account the compaction geometry, $\rho_0 = 0.6$ is the initial relative density of the compact. The final-stage densification rate is given by:

$$\dot{\rho} = \frac{3}{2} \cdot C \cdot \frac{\rho \cdot (1-\rho)}{\left(1-(1-\rho)^{1/n}\right)^n} \cdot \left(\frac{3 \cdot B_f \cdot \sigma}{2 \cdot n}\right)^n \quad , \tag{4}$$

where the constant $B_f = 1.8$[13] is related to the stress state in the die.

Since there is no fundamental change of the densification mechanism with the addition of reinforcement ceramic powder such as TiC[7] and ZrO_2[13] to the titanium powders, Eqs. (3) and (4) can still be used for modeling the densification process in composite blends, although a knock-down factor (f) multiplies the right-hand expression in these equations to take into account the reduced densification kinetics of metal/ceramic blends discussed in Sec. IV. A, as well as possible die/piston friction effects. Comparisons between calculations using Eq. (3) and experimental observations are shown in Fig. 6 for Ti-10 vol% TiC at 870 °C[7] with a knock-down factor $f = 0.14$, and Ti-10 vol% ZrO_2 at 980 °C[13] with $f = 0.33$ at 1 MPa and $f = 0.24$ at 3 MPa. The knock-down factor for Ti-10 vol% TiC is similar to that used[37] to model densification of pure titanium. However, the knock-down factor decreased in Ti-10% ZrO_2 with respect to pure titanium hot pressing at 980 °C at both 1 MPa ($f = 1$) and 3 MPa ($f = 0.6$).

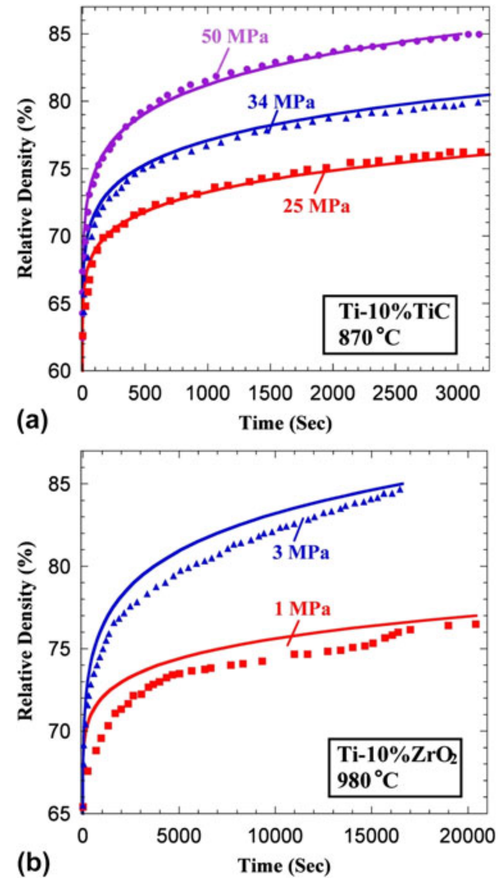

FIG. 6. Comparison between continuum modeling [solid lines, calculated from Eq. (3)] and densification measurements (symbols, from experimental measurements reported in Refs. 7,13) for (a) Ti-10 vol% TiC at 870 °C and (b) Ti-10 vol% ZrO_2 at 980 °C.

Similar comparisons between continuum modeling and densification measurements are shown in Fig. 7 for the present Ti-6Al-4V/TiC composite. The knock-down factors at 10 MPa [Fig. 7(a)] are $f = 1$, 0.67 and 0.46 for 0, 14 and 26 vol% TiC respectively. At 20 MPa, the knock-down factors are $f = 0.77$ and 0.47 for 0 and 14 vol% TiC [Fig. 7(b)].

C. Finite element simulation of Ti-6Al-4V/TiC densification

FE simulations to describe the densification of the present Ti-6Al-4V/TiC composite were conducted following the methods described in detail in Ref. 37 for two configurations with periodic boundary conditions, simulating an infinite array of spherical powders: face-centered cubic (fcc) with four 1/8 spheres of the same radius in the unit

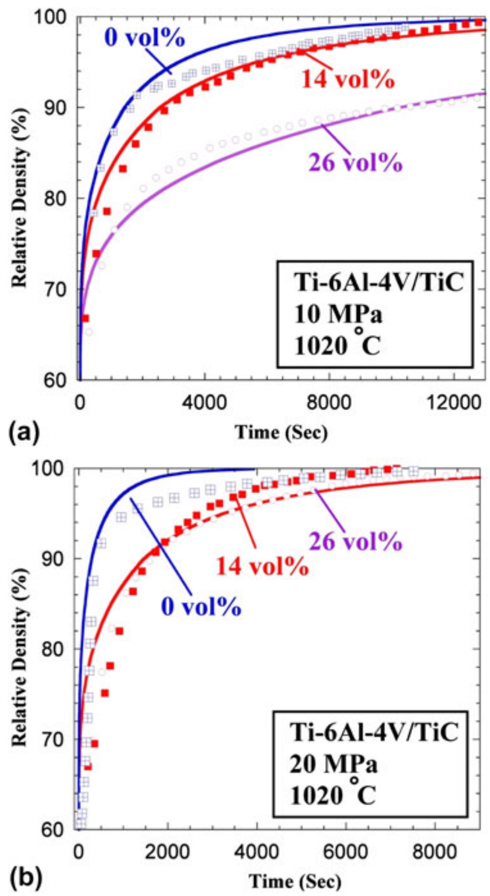

FIG. 7. Comparison between continuum modeling [solid lines, calculated from Eq. (3)] and densification measurements (symbols) for Ti-6Al-4V with 0, 14 and 26 vol% TiC densified at 1020 °C at pressures of (a) 10 MPa and (b) 20 MPa.

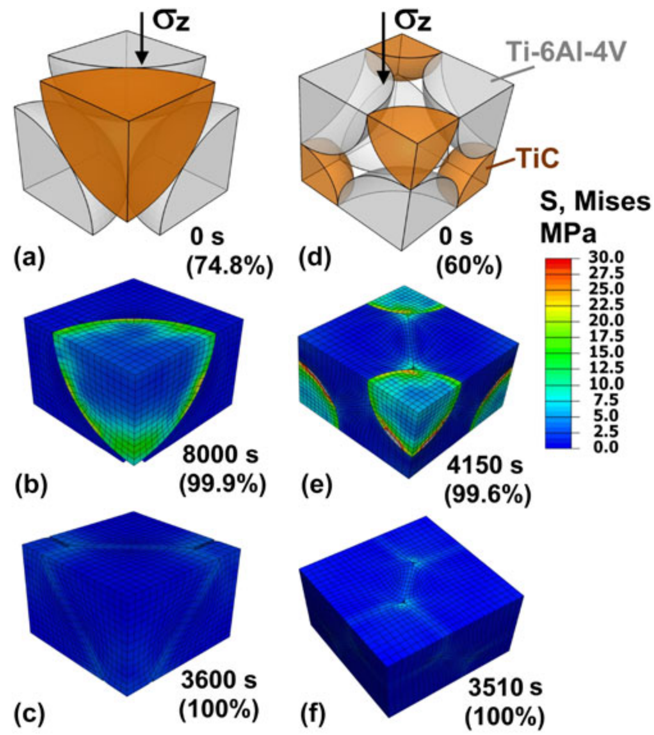

FIG. 8. FE simulation of Ti-6Al-4V/TiC powder composite densification with the fcc configuration: (a, b) initial and densified states of Ti-6Al-4V with 25 vol% TiC, (c) Densified state of Ti-6Al-4V without TiC. Same with the sc configuration: (d, e) initial and densified states of Ti-6Al-4V with 20 vol% TiC, (f) densified state of Ti-6Al-4V without TiC.

cell, and simple cubic (sc) with eight 1/8 spheres with two radii in the unit cell [Figs. 8(a) and 8(d)]. In the fcc configuration with an initial packing density of 74.8%, three of the spheres are Ti-6Al-4V and one is TiC, the volume fraction of which is thus 25% [Fig. 8(a)]. In the sc configuration, the diameter of spherical TiC spheres was 63.4% of that of the Ti-6Al-4V spheres, so that the initial packing density was 60% and the TiC volume fraction is 20% [Fig. 8(d)], close to the experimental values. Given the low applied stress and low temperature (as compared to the TiC melting point) used during powder composite densification, it was assumed that TiC was elastic with a Young's modulus of 450 GPa and Poisson's ratio of 0.2.[38] The Ti-6Al-4V powders were assumed to deform by transformation-mismatch plasticity [Eq. (2)]. For thermal cycling with a 860–1020 °C temperature range and a 191 s cycle duration, Eq. (2) reduces to Eq. (1) with $n = 1$ and $C = 1.045 \times 10^{-5}$ MPa/sec. This creep type behavior was modeled as the rate-dependent plasticity via the "static" procedure in ABAQUS/Standard 6.7–3 (Dassault Systemes, Vélizy-Villacoublay, France). For fast convergence rather than via the "visco" procedure, as described in more detail in Ref. 37. The densified or deformed state of the unit cells is shown in Figs. 8(b) and 8(e). The plastic matrix flow around the elastic TiC particles during densification and load transfer [visible as regions of higher stress in the particles in Figs. 8(b) and 8(e)] takes place from the compliant, plastic matrix to the stiff, elastic particles. Load transfer is nearly absent at the end of densification when the composite is under near perfect hydrostatic pressure conditions [Figs. 8 (c) and 8(f)], but the lack of deformation of the TiC particles leads to incomplete densification at the triple line where one TiC and two deformed Ti-6Al-4V spheres meet. By contrast, when all powders in the unit cell are plastically deforming Ti-6Al-4V, the powders deform uniformly and have faster densification kinetics, as reported in Ref. 37.

FE simulation results for powder densification kinetics are shown in Fig. 9(a) for the fcc configuration under an applied stress of 10, 15, and 20 MPa and in Fig. 9(b) for the sc configuration under 10 and 20 MPa. A comparison of densification curves between Ti-6Al-4V with and without TiC shows that densification becomes faster with the increasing applied stress and slower with the

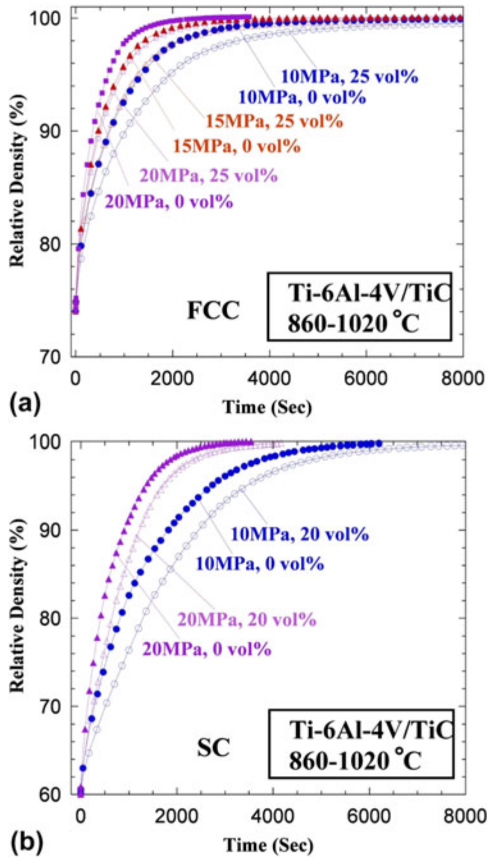

FIG. 9. Densification kinetics of Ti-6Al-4V and Ti-6Al-4V/TiC powder composites as determined by FE simulations: (a) fcc configuration (0 and 25 vol% TiC) with an applied stress of 10, 15, and 20 MPa and (b) sc configuration (0 and 20 vol% TiC) with an applied stress of 10 and 20 MPa.

addition of TiC. At 20 MPa, 99.8% relative density is predicted after 50 min for Ti-6Al-4V and after 69 min for Ti-6Al-4V/20TiC for the sc configuration, and after 44 and 137 min, respectively, for Ti-6Al-4V/25TiC in the fcc configuration. These values are similar to those measured experimentally for Ti-6Al-4V [35 min, Fig. 3(b)] and Ti-6Al-4V/25TiC [147 min, Fig. 3(b)]. Thus, despite the drastic simplifications used, the FE model can provide semi-quantitative predictions for the densification kinetics of metal and metal/ceramic powder blends. More complex models capturing the non-spherical shape, the size distribution and the non-periodic distribution of powders are needed for improved results.

Significant differences between pure Ti-6Al-4V powders and the blends of TiC and Ti-6Al-4V powders in densification kinetics are found for a relative density >99% from different densification states due to the lack of synergy in TiC and Ti-6Al-4V [Figs. 8(c) and 8(f) and Fig. 3]. This may partially explain the insignificant difference in densification kinetics with respect to different TiC compositions at a specified load (Fig. 3).

V. CONCLUSIONS

The densification kinetics of Ti-6Al-4V/TiC powder blends were measured under hot pressing conditions for various TiC powder volume fractions, applied external stresses and temperature schedules (thermal cycling or isothermal). The following main conclusions are reached:

(1) Densification kinetics increases with applied external stress in both thermal cycling and isothermal conditions.

(2) Under isothermal conditions, the addition of 14 vol% TiC powder does not affect densification appreciably. However, when the TiC volume fraction reaches 26 vol%, densification is strongly delayed.

(3) Under thermal cycling conditions, densification rates were similar for TiC volume fractions of 7–26% although they were much slower than pure Ti-6Al-4V without TiC additions.

(4) General agreement is found between experimental measurements of densification kinetics, models using a continuum approach and simulation by the finite-element method with powder-level FE.

ACKNOWLEDGMENT

This research was supported by a grant from the Boeing Corp.

REFERENCES

1. R.R. Boyer: An overview on the use of titanium in the aerospace industry. *Mater. Sci. Eng., A* **213**(1–2), 103 (1996).
2. M. Geetha, A.K. Singh, R. Asokamani, and A.K. Gogia: Ti based biomaterials, the ultimate choice for orthopaedic implants - a review. *Prog. Mater. Sci.* **54**(3), 397 (2009).
3. S. Abkowitz: Titanium: From jets to biomedical devices. *Adv. Mater. Process.* **163**(7), 53 (2005).
4. S. Abkowitz, S. Abkowitz, H. Fisher, and P. Schwartz: CermeTi® discontinuously reinforced Ti-matrix composites: Manufacturing, properties, and applications. *JOM.* **56**(5), 37 (2004).
5. H. Choe, S. Abkowitz, and S.M. Abkowitz: Influence of processing on the mechanical properties of Ti-6Al-4V-based composites reinforced with 7.5 mass% TiC and 7.5 mass% W. *Mater. Trans.* **49**(9), 2153 (2008).
6. J. Lu, J. Qin, Y. Chen, Z. Zhang, W. Lu, and D. Zhang: Superplasticity of coarse-grained (TiB+TiC)/Ti-6Al-4V composite. *J. Alloys Compd.* **490**(1–2), 118 (2010).
7. N. Taylor, D.C. Dunand, and A. Mortensen: Initial stage hot pressing of monosized Ti and 90% Ti-10% TiC powders. *Acta Mater.* **41**(3), 955 (1993).
8. C. Yolton: The pre-alloyed powder metallurgy of titanium with boron and carbon additions. *JOM* **56**(5), 56 (2004).
9. S. Ranganath: A review on particulate-reinforced titanium matrix composites. *J. Mater. Sci.* **32**(1), 1 (1997).
10. D.S. Wilkinson and M.F. Ashby: Pressure sintering by power law creep. *Acta Metall. Mater.* **23**(11), 1277 (1975).
11. E. Arzt, M. Ashby, and K. Easterling: Practical applications of hotisostatic pressing diagrams: Four case studies. *Metall. Mater. Trans. A.* **14**(1), 211 (1983).
12. A.S. Helle, K.E. Easterling, and M.F. Ashby: Hot-isostatic pressing diagrams: New developments. *Acta Metall. Mater.* **33**(12), 2163 (1985).

13. C. Schuh, P. Noel, and D.C. Dunand: Enhanced densification of metal powders by transformation-mismatch plasticity. *Acta Mater.* **48**(8), 1639 (2000).
14. C. Schuh and D.C. Dunand: Non-isothermal transformation-mismatch plasticity: Modeling and experiments on Ti-6Al-4V. *Acta Mater.* **49**(2), 199 (2001).
15. B. Ye, M.R. Matsen, and D.C. Dunand: Enhanced densification of Ti-6Al-4V powders by transformation-mismatch plasticity. *Acta Mater.* **58**(11), 3851 (2010).
16. G.W. Greenwood and R.H. Johnson: The deformation of metals under small stresses during phase transformations. *Philos. Trans. R. Soc. London, Ser. A* **283**(1394), 403 (1965).
17. P. Zwigl and D. Dunand: Transformation superplasticity of zirconium. *Metall. Mater. Trans. A.* **29**(10), 2571 (1998).
18. D.C. Dunand, C. Schuh, and D.L. Goldsby: Pressure-induced transformation plasticity of H_2O ice. *Phys. Rev. Lett.* **86**(4), 668 (2001).
19. C.A. Schuh and D.C. Dunand: Enhanced densification of zinc powders through thermal cycling. *Acta Mater.* **50**(6), 1349 (2002).
20. J.M. Ottino and R.M. Lueptow: Material science: On mixing and demixing. *Science* **319**(5865), 912 (2008).
21. D. Shi, A.A. Abatan, W.L. Vargas, and J.J. McCarthy: Eliminating segregation in free-surface flows of particles. *Phys. Rev. Lett.* **99**(14), 148001 (2007).
22. Q. Li, E. Chen, D. Bice and D. Dunand: Transformation superplasticity of cast titanium and Ti-6Al-4V. *Metall. Mater. Trans. A* **38**(1), 44 (2007).
23. H.J. Frost and M.F. Ashby: *Deformation-Mechanism Maps: The Plasticity and Creep of Metals and Ceramics*, 1st ed. (Pergamon Press, Oxford, UK, 1982).
24. C. Schuh and D.C. Dunand: An overview of power-law creep in polycrystalline β-titanium. *Scr. Mater.* **45**(12), 1415 (2001).
25. J. Zhu, P. Liaw, J. Corum, and H. McCoy: High-temperature mechanical behavior of Ti-6Al-4V alloy and TiC p/Ti-6Al-4V composite. *Metall. Mater. Trans. A.* **30**(6), 1569 (1999).
26. M. Daymond, C. Lund, M. Bourke and D. Dunand: Elastic phase-strain distribution in a particulate-reinforced metal-matrix composite deforming by slip or creep. *Metall. Mater. Trans. A.* **30**(11), 2989 (1999).
27. D.C. Dunand and S. Myojin: Biaxial deformation of Ti-6Al-4V and Ti-6Al-4V/TiC composites by transformation-mismatch superplasticity. *Mater. Sci. Eng., A* **230**(1–2), 25 (1997).
28. P. Zwigl and D. Dunand: Transformation superplasticity of iron and Fe/TiC metal matrix composites. *Metall. Mater. Trans. A.* **29**(2), 565 (1998).
29. C. Schuh and D.C. Dunand: Whisker alignment of Ti-6Al-4V/TiB composites during deformation by transformation superplasticity. *Int. J. Plast.* **17**(3), 317 (2001).
30. C. Schuh and D.C. Dunand: Load transfer during transformation superplasticity of Ti-6Al-4V/TiB whisker-reinforced composites. *Scr. Mater.* **45**(6), 631 (2001).
31. M. Frary, C. Schuh, and D.C. Dunand: Kinetics of biaxial dome formation by transformation superplasticity of titanium alloys and composites. *Metall. Mater. Trans. A.* **33**(6), 1669 (2002).
32. J. Besson and A.G. Evans: The effect of reinforcements on the densification of a metal powder. *Acta Metall. Mater.* **40**(9), 2247 (1992).
33. C.L. Martin and D. Bouvard: Study of the cold compaction of composite powders by the discrete element method. *Acta Mater.* **51**(2), 373 (2003).
34. L. Olmos, C.L. Martin, and D. Bouvard: Sintering of mixtures of powders: Experiments and modelling. *Powder Technol.* **190**(1–2), 134 (2009).
35. J.F. Shackelford and W. Alexander: *CRC Materials Science and Engineering Handbook*, 3rd ed. (CRC Press, Boca Raton, FL, 2000).
36. O.J. Dura, E. Bauer, L. Vazquez, and M.A. Lopez de la Torre: Depressed thermal conductivity of mechanically alloyed nanocrystalline 10 mol% yttria-stabilized zirconia. *J. Phys. D.* **43**(10), 105407 (2010).
37. B. Ye, M. Matsen, and D. Dunand: Finite-element modeling of titanium powder densification. *Metall. Mater. Trans. A.* **43**(1), 381 (2012).
38. R. Chang and L.J. Graham: Low-temperature elastic properties of ZrC and TiC. *J. Appl. Phys.* **37**(10), 3778 (1966).